Numerical simulation of angular structure of the near-horizon sky brightness in ground-based observations. Part 3. Regularities of angular distribution

S.M. Sakerin, T.B. Zhuravleva, and I.M. Nasrtdinov

Institute of Atmospheric Optics,
Siberian Branch of the Russian Academy of Sciences, Tomsk

Received August 9, 2004

Regularities in formation of the spatial-angular structure of clear-sky brightness in atmospheric windows in the visible and near-IR spectral regions at large zenith viewing angles are discussed. It is shown based on computer simulation that the angular dependences of brightness components caused by single and multiple scattering behave similarly, but the latter has much less elongation (smoothes the angular dependence). In the azimuth dependence of the diffuse radiation, the main variability (5–10 times and more) is observed in the forward hemisphere because of the priority effect of the single scattering and the aerosol scattering phase function having the pronounced forward peak. The angular behavior in the backward hemisphere is determined by the multiply scattered component and the molecular scattering. The less asymmetric multiple component of sky brightness has a weak and almost linear dependence on the forward peak of the aerosol scattering phase function. The zenith distributions of the sky brightness have a maximum in the near-horizon zone. The characteristics of this maximum depend on the atmospheric turbidity: with the increase of the optical depth, the brightness maximum shifts toward the horizon. As approaching the horizon, the zenith dependences of brightness converge asymptotically to the value of the source function due to the brightness saturation of the surface haze.

Introduction

As is known, investigations of brightness fields of the clear daylight sky observed from the ground have been conducted mainly for zenith angles under ~75° in the visible spectral region, where the gas absorption is low. Among most general regularities of the spatial structure, the increase in sky brightness at shortening of the angular distance to the Sun and at approaching the horizon were noted.[1–4] According to our data, no detailed investigations of the near-horizon sky in the IR spectral region have been performed because of cumbersome calculations connected with accounting for the atmospheric sphericity and molecular absorption.

In Parts 1 and 2 of our work[5,6] we presented the algorithm of numerical modeling of scattered radiation in the spherical cloudless atmosphere with allowance for multiple scattering, molecular absorption, and instrumental functions of photometers involved in the radiation experiments. Calculations of radiation, performed for the atmospheric transparency windows of 0.50, 0.87, 1.245, and 2.137 μm, two experimental geometries (solar almucantar and horizon), and typical atmospheric conditions have shown that disregard to absorption leads to ~2–40% errors depending mostly on the slant optical absorption thickness in the observation direction. With the example of the 0.5 μm spectral channel, we have studied the influence of the aerosol optical thickness (AOT) of the atmosphere and the aerosol single scattering albedo Λ^{aer} on the sky brightness. It has been demonstrated that the sky brightness in the forward hemisphere (in the Sun-oriented direction) can have a nonmonotonic dependence on AOT with a maximum in the range 0.03–0.15. Scattered radiation in the backward hemisphere decreases monotonically with the increase of AOT for all atmospheric conditions. Dependence of sky brightness on the single scattering albedo is almost linear (increase in brightness with the growth of Λ^{aer}) and has a greater influence on the radiation caused by the multiple scattering.

In this paper, we proceed with the analysis of the model calculations of the sky brightness field concerning dependences of radiation on the viewing zenith and azimuth angles. Since the applied algorithms and aerosol model have been already described,[5,6] we restrict ourselves to listing the input parameters, at which most calculations were performed:

1) Solar zenith angles ξ = 60, 75, 85°;

2) Viewing (detector) zenith angles, ξ from 60 to 90°;

3) Viewing azimuth angles φ with respect to the Sun: 0, 20, 30, 90, 180°;

4) Underlying surface albedo A_S = 0.2.

Recall that temperature, pressure, and gas concentration (H_2O, CO_2, etc.) profiles were set according to the AFGL model for the mid-latitude summer.[7] Unlike Ref. 6, in this work, all calculations are given only for the aerosol-gaseous atmosphere and

0235-6880/05/03 222-10 $02.00 © 2005 Institute of Atmospheric Optics

with allowance for the instrumental spectral functions, that is why to simplify the sky brightness indications, the subscript $\Delta\lambda$ and superscript AG are omitted. To elucidate the regularities, besides the sky brightness itself $B(\xi; \varphi)$, we will consider the components conditioned by the single $B_o(\xi; \varphi)$ and multiple $B_m(\xi; \varphi)$ scattering. To make the analysis more convenient, the azimuth distributions of sky brightness are presented as dependent on the scattering angle θ, which is in a simple relation with the experimental geometry:

$$\cos\theta = \sin\xi \sin\xi \cos\varphi + \cos\xi \cos\xi . \quad (1)$$

1. General properties

Let us cite the equation for sky brightness in approximation of the single scattering and the plane-parallel atmosphere model,[1,6] which will be useful for further analysis:

$$B_o(\xi,\varphi) = E_o g^{atm}(\theta)\Lambda^{atm}\frac{M}{M-m}[T^{atm}(m) - T^{atm}(M)] =$$

$$= E_o \frac{g^{\Lambda}(\theta)\tau^{\Lambda}_{sca} + g^{R}(\theta)\tau^{R}}{\tau^{\Lambda}_{sca} + \tau^{R}} \frac{\tau^{\Lambda}_{sca} + \tau^{R}}{\tau^{\Lambda} + \tau^{R} + \tau^{G}} \frac{M}{M-m} \times$$

$$\times\{T^{G}(m)\exp[-(\tau^{\Lambda}+\tau^{R})m] - T^{G}(M)\exp[-(\tau^{\Lambda}+\tau^{R})M]\} =$$

$$= E_o \frac{[g^{\Lambda}(\theta)\tau^{\Lambda}_{sca} + g^{R}(\theta)\tau^{R}]M}{(\tau^{\Lambda} + \tau^{R} + \tau^{G})(M-m)} \times$$

$$\times\left\{T^{G}(m)\exp[-(\tau^{\Lambda} + \tau^{R})m] - T^{G}(M)\exp[-(\tau^{\Lambda} + \tau^{R})M]\right\}, \quad (2)$$

where E_o is the off-atmospheric solar constant (illuminance); $g^{atm}(\theta)$ is the scattering phase function of atmospheric thickness dependent on the aerosol and molecular scattering phase functions; $m(\xi)$, $M(\xi)$ are optical masses of the atmosphere at the solar and viewing zenith angles, respectively; T^{atm}, T^{G} are transmittances of the atmosphere and its gas component; Λ^{atm} is the single scattering albedo of the atmospheric medium; τ^{R}, τ^{G} are optical thicknesses of molecular scattering and absorption; τ^{Λ}, τ^{Λ}_{sca} are the aerosol optical thicknesses of extinction and scattering.

The actually observed sky brightness (with allowance for the multiple scattering) has a more complex dependence on the atmospheric characteristics and geometry. At the same time, as was noted in Refs. 1 and 8, to describe the virtual brightness, we may use the equation qualitatively similar to Eq. (2), through substituting the scattering phase function of the atmospheric thickness to the phase function of sky brightness. As for the influence of atmospheric sphericity, it does not affect the general regularities of the sky brightness formation, but introduces some quantitative differences in situations at $\tau^{\Lambda} < 0.1$ and/or $\xi > 82°$ (Ref. 5). That is, for the qualitative analysis of the influence of different factors on the sky brightness, it is quite possible to use Eq. (2), which gives a pictorial view on redistribution of the role of atmospheric optical characteristics at variations of the observational geometry.

In the limiting case ($\xi = 90°$, $M \to \infty$), the atmospheric scattering column is within the limits of the horizontal near-surface layer, and Eq. (2) takes the form:

$$B_o(90,\varphi) = E_o g_0^{atm}\Lambda_0^{atm} T^{G}(m)\exp[-(\tau^{\Lambda} + \tau^{R})m], \quad (3)$$

where

$$g_0^{atm} = \frac{g_0^{\Lambda}(\theta)\sigma_0^{\Lambda} + g_0^{R}(\theta)\sigma_0^{R}}{\sigma_0^{\Lambda} + \sigma_0^{R}} \text{ and } \Lambda_0^{atm} = \frac{\sigma_0^{\Lambda} + \sigma_0^{R}}{\varepsilon_0}$$

are the phase function and albedo of the single scattering in the surface layer; σ_0^{Λ}, σ_0^{R} are the coefficients of aerosol and molecular scattering; ε_0 is the general extinction coefficient; $m \approx 1/\cos\xi$.

Note that Eq. (3) separates optical characteristics of the atmosphere: the first two factors g^{atm} and Λ^{atm} are referred to the surface layer (do not depend on the vertical stratification) and characterize its scattering capacity as that of a secondary radiation source, while the last two factors determine the direct radiation attenuation by the whole atmospheric thickness.

As yet, avoiding the angular dependences, let us summarize the influence of main factors on the total level of scattered radiation. It follows from the results of previous investigations[5,6] that the diffuse radiation: a) decreases with the increase of absorption (decrease of the atmospheric albedo Λ^{atm}); b) may have a non-monotonic dependence on the atmospheric AOT. In the spectral dependence, sky brightness must follow (other things being equal) the changes in the solar constant, that is, when $\lambda > 0.5$ μm, the intensity of sky brightness decreases with the growth of wavelength (see Fig. 1).

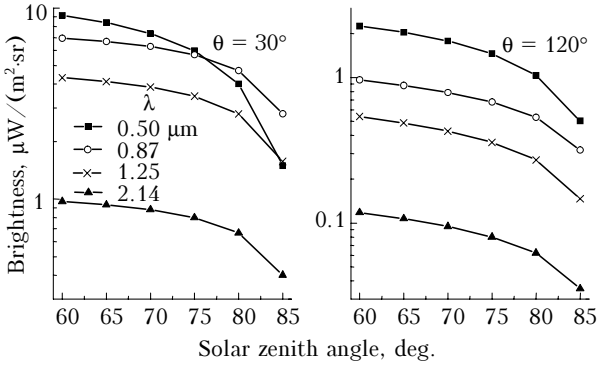

Fig. 1. Dependences of sky brightness on the zenith angle ξ in different spectral regions for the scattering angles θ = 30 and 120° (ξ = 90°; τ^{Λ} = 0.1).

Besides, Fig. 1 illustrates the changes in sky brightness near the horizon depending on the angle ξ . To exclude the influence of the scattering phase function, calculations in this case were performed for fixed values of θ. The results show that with the increase of the solar zenith angle, the sky brightness

gradually decreases, most intensively in the region $\xi > 80°$. This regularity is easy to explain using the example of the single scattering component (3). At a fixed θ, the brightness change is determined by almost exponential fall of the atmospheric transmittance (atmospheric transparency). In other words, with the growth of the solar zenith angle, the sighted atmospheric column is illuminated by still weaker radiation. It is obvious that the brightness decrease intensifies with the increase of the total optical thickness $\tau = \tau^R + \tau^G + \tau^A$.

From Fig. 2, we can judge the contribution of the single and multiple scattering into sky brightness at different ξ.

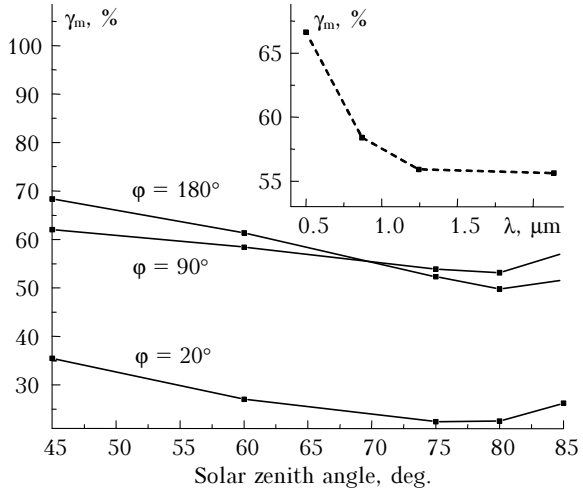

Fig. 2. The contribution of the multiple scattering $\gamma_m(\xi)$ at different observation azimuths ($\lambda = 0.87$ μm, $\tau^A = 0.1$); the inset shows an example of spectral dependence γ_m ($\varphi = 90°$; $\xi = 60°$; $\xi = 90°$).

With the growth of the solar zenith angle, the contribution of the multiple scattering $\gamma_m = B_m/(B_o + B_m)$ shows the tendency of reducing with a minimum at about $\xi \approx 80°$. The character of this dependence can be explained mainly by the change of the single component $B_o(\xi)$ under the influence of two factors: a) growth of the scattering phase function with the decrease of θ and b) rapid transparency decrease in the region $\xi > 80°$ (see above).

Taking into account that the brightness component $B_m(\xi; \varphi)$ has a slight asymmetry as compared to $B_o(\xi; \varphi)$, redistribution of their influence with the change of the scattering angle can be judged by the singly scattered radiation that depends on $g^{atm}(\theta)$. It follows from Eq. (2) that the angular behavior of the atmospheric scattering phase function $g^{atm}(\theta)$ results from the change of the aerosol scattering characteristics as compared to the molecular scattering: the growth of the aerosol scattering phase function g^A with respect to g^R or of the ratio τ^A/τ^R automatically leads to the growth of the single component B_o and reduction of γ_m. In the aureole angles, the aerosol scattering phase function due to its pronounced elongation (large values) has a dominant role ($g^{atm} \to g^A$), the contribution of the single scattering is maximal, and the intensity of γ_m is below 35% (see $\varphi = 20°$ in Fig. 2). At large azimuth angles, the influence of the multiple scattering gradually increases (following the slope of $g^A(\theta)$), but does not exceed 60–70%.

By analyzing the data in Table 1 we can judge the influence of other factors on γ_m (except for the dependence on φ and ξ).

Table 1. The influence of aerosol characteristics (τ^A, G^A) on γ_m at $\xi = 80°$ and $\varphi = 0, 90, 180°$

λ, μm	G^A	τ^A	φ, °		
			0	90	180
0.5	5.3	0.1	17.6	56.3	62.8
		0.2	27.0	69.7	77.5
	8.3	0.03	14.7	51.6	41.1
		0.1	21.0	69.3	63.6
		0.4	50.7	92.5	91.2
	9.7	0.1	17.0	65.6	69.5
		0.2	26.6	78.0	83.0
0.87	8	0.03	7.8	31.5	26.6
		0.2	26.8	67.6	63.7
2.14	11.1	0.03	9.5	35.3	33.6
		0.1	22.6	54.4	51.2

At variations of τ^A and the degree of elongation of the aerosol scattering phase function in the actual variability range, the maximal influence on the redistribution of the multiple and single scattering contributions is mainly determined by the atmospheric AOT:

– with the increase in τ^A, the magnitude of γ_m grows two or three times in the whole range of the angles φ;

– dependence of γ_m on the scattering phase function elongation (G^A) is nonlinear and weak enough (for $\tau^A_{0.5} = 0.1$ the change in γ_m is about 20–30%).

Summarizing, we conclude that the least contribution of multiple scattering into diffuse radiation ($\gamma_m \sim 0$–20%) will be observed in the aureole area of angles (φ and $|\xi - \xi| \to 0$), at small values of the atmospheric AOT, and in the longwave spectral region. Decrease of γ_m with the increase in wavelength takes place because of spectral dependence of the optical thicknesses $\tau^R(\lambda)$, $\tau^A(\lambda)$ and the corresponding transformation of $g^{atm}(\theta)$.

The inset in Fig. 2 illustrates the character of reduction of the multiple scattering percentage with the wavelength growth at a typical spectral dependence of optical thicknesses $\tau^A \approx 0.06\lambda^{-1.3}$; $\tau^R \approx 0.009\lambda^{-4}$. The "stabilization" $\gamma_m(\lambda) \to$ const results from the fact that in the region above 1 μm the molecular scattering becomes negligible, and the sky brightness field is determined only by the aerosol characteristics $g^A(\theta)$ and τ^A. In this spectral region, the influence of fine-disperse aerosol ($r < 0.5$ μm) on the scattering is also reduced. Therefore, we can amend: the diffuse radiation in the region greater than ~1 μm as well as the portion of multiple scattering are determined mainly by the properties of large aerosol particles.

2. Azimuth dependence of sky brightness

Features of the angular structure of diffuse radiation reflect the redistribution of the role of the single and multiple scattering, as well as the phase functions of the aerosol and molecular scattering. Note that at a full sweep of azimuth distributions of the sky brightness $B(\varphi = 0–180°)$, in different almucantars a limited range of the scattering angles θ is realized, which varies with variation of the zenith angle ξ . Therefore, to make the comparison with the scattering phase functions more convenient, here and further we present azimuth distributions of sky brightness in the form of the scattering angle dependences $B(\theta)$. If necessary, the brightness can be easily recalculated from the angles θ into φ by Eq. (1).

Maximal influence on the sky brightness asymmetry is exerted by the single component $B_o(\theta)$ and the aerosol scattering phase function $g^A(\theta)$ (Figs. 3*a* and *b*).

It follows from Eq. (2) that in case of azimuth dependence (with fixed M and m) $B_o(\theta)$ coincides with the scattering phase function $g^{atm}(\theta)$ accurate to the constant. The multiple scattering component $B_m(\theta)$ is less asymmetric, but its elongation also monotonically grows (lessens) following g^{atm}, as will be shown below. Hence, Eq. (2), for the single component, qualitatively correctly reflects the basic regularities of formation of the angular structure of sky brightness and allows us to analyze the effects of different factors.

As is known, aerosol scatters mainly into the forward hemisphere. If we use the asymmetry factor

$$G = \int_0^{\pi/2} g(\theta)\sin\theta\,d\theta \Big/ \int_{\pi/2}^{\pi} g(\theta)\sin\theta\,d\theta, \qquad (4)$$

in order to quantitatively characterize the differences between the scattering phase functions g^A and g^R, then for molecular scattering $G^R = 1$, while for aerosol the asymmetry of the scattering phase function is much more: $G^A \approx 3–11$ (Ref. 8). That is, the effect of aerosol is in increase of the sky brightness anisotropy, while the effect of molecular scattering is inverse. Due to strong elongation of $g^A(\theta)$ and fulfillment of the requirement $\tau^A \geq \tau^R$ (for most part of the considered spectral region), the basic regularity of the angular distribution is a significant increase in scattered radiation, when shortening the angular distance to the Sun. As moving away from the solar vertical, the influence of the scattering phase function $g^R(\theta)$ becomes stronger, the contribution of the multiple scattering simultaneously grows and, following from these two factors, the sky brightness phase function $B(\theta)$ becomes smoother. The point of redistribution of the role of aerosol and molecular scattering (Fig. 3*a*), as well as single and multiple (Fig. 3*b*) one lies in the range $\theta \approx 60°$. When optical thickness τ^R is comparable to τ^A (visible range), the diffuse radiation in the backward hemisphere is mainly influenced by the molecular scattering phase function $g^R(\theta)$.

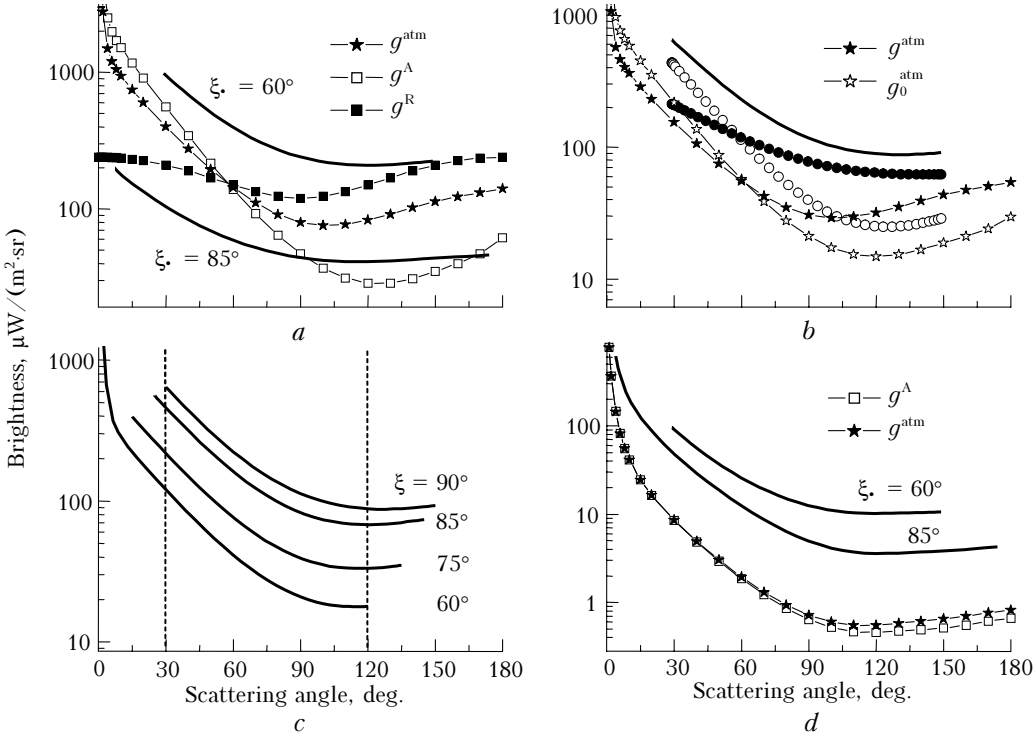

Fig. 3. Azimuth distributions of sky brightness (as the function of the angle θ) (— for B, ○ for B_o, • for B_m): for the zenith angles ξ = 60 and 85° (ξ = 90°, λ = 0.5 μm, τ^A = 0.2) as compared to the scattering phase functions g^{atm}, g^A, g^R (*a*); individually for the brightness components B_o and B_m (ξ = 90°, ξ = 60°, λ = 0.87 μm, τ^A = 0.2) as compared to the scattering phase functions g^{atm}, g_0^{atm} (*b*); for different almucantars of ξ = 60–90° (ξ = 60°, λ = 0.87 μm, τ^A = 0.2) (*c*); the same as (*a*), but in the infrared spectral region (λ = 2.14 μm, τ^A = 0.1) (*d*).

Note that for the horizontal direction ($\xi = 90°$), according to Eq. (3), the angular behavior of $B_o(\theta)$ does follow the surface scattering phase function g_0^{atm} (see Fig. 3*b*), which is more asymmetric as compared to g^{atm}. Stronger elongation of $B(\theta)$ at $\xi \to 90°$ is the result of much greater relative contribution of the surface aerosol scattering $\sigma_0^A / \sigma_0^R \gg \tau^A / \tau^R$.

On the whole, angular dependences of sky brightness at different almucantars (Fig. 3*c*) are identical. The distinction refers to different levels of diffuse radiation and the range of the scattering angles θ, which can be realized at variations of the viewing zenith angle ξ. Within one range of the scattering angles (see dashed boundaries in Fig. 3*c*), the sky brightness asymmetry $B(\theta)$ intensifies with approaching the horizon.

Transformation of the angular dependence $B(\theta)$ at a change of the spectral region (compare Figs. 3*a* and *b*) follows from the dependence of the atmospheric scattering phase function on the relative characteristic τ^A/τ^R. Since $\tau^R \sim \lambda^{-4}$ and $\tau^A \sim \lambda^{-1}$, the increase in wavelength leads to redistribution of the roles of scattering components: atmospheric and aerosol scattering phase functions approach ($g^{atm} \to g^A$) and, simultaneously, the role of the single scattering grows, and the scattering phase function of the sky brightness elongates further. In the longwave part of the spectral region ($\lambda > 1$ μm), the molecular scattering becomes negligible, $g^{atm}(\theta) \approx g^A(\theta)$, and the sky brightness over the whole range of scattering angles is determined by the aerosol characteristics τ^A and $g^A(\theta)$ only.

As for features of the azimuth behavior of $B(\varphi)$ at different solar zenith angles, we can state the following. At large zenith angles (see $\xi = 85°$ in Fig. 3*d*), sky brightness measurements cover the aureole region, which results in increase of asymmetry and dependence of $B(\theta)$ (in the forward hemisphere) on the elongation of the aerosol scattering phase function. With decrease of ξ (and, as a result, of the range of θ), angular distributions $B(\theta)$ come closer both in the forward and backward hemispheres irrespective of $g^A(\theta)$. Summarizing the analysis of the spectral dependence and influence of the solar zenith angle on sky brightness, we conclude that the increase of ξ and λ raises the role of the single scattering, intensifies the elongation of $B(\varphi)$ and its sensitivity to variations of the scattering phase function $g^A(\theta)$.

Above we have already emphasized an important role of the aerosol scattering phase function in formation of the angular structure of sky brightness. Estimate now quantitatively how the change in the $g^A(\theta)$ elongation affects the asymmetry of the angular behavior of $B(\theta)$. To set different aerosol scattering phase functions, we invoke the Henyey-Greenstein model approximation.[9] It is not quite correct to compare elongations of scattering phase functions $g^A(\theta)$ and sky brightness $B(\theta)$ by Eq. (4): the range θ for the scattering phase functions is $[0 - \pi]$, whereas in the azimuth brightness dependence (its single component, if to be more precise) only the scattering angles from $(\xi - \xi_\odot)$ to $(\xi + \xi_\odot)$ are realized. Therefore, we evaluate this relation using the truncate asymmetry factors:

$$G^*(g^A) = \int_{\xi-\xi_\odot}^{\pi/2} g(\theta)\sin\theta\,d\theta \Big/ \int_{\pi/2}^{\xi+\xi_\odot} g(\theta)\sin\theta\,d\theta,$$
$$G^*(B) = \int_{\xi-\xi_\odot}^{\pi/2} B(\theta)\sin\theta\,d\theta \Big/ \int_{\pi/2}^{\xi+\xi_\odot} B(\theta)\sin\theta\,d\theta. \quad (5)$$

Simulation results have shown (Fig. 4*a*, curves *1* and *2*) that in the actual variability range of the aerosol scattering phase functions, the truncate asymmetry factors $G^*(B)$ and $G^*(B_m)$ have almost linear and relatively weak dependence on $G^*(g^A)$ for different λ and τ^A.

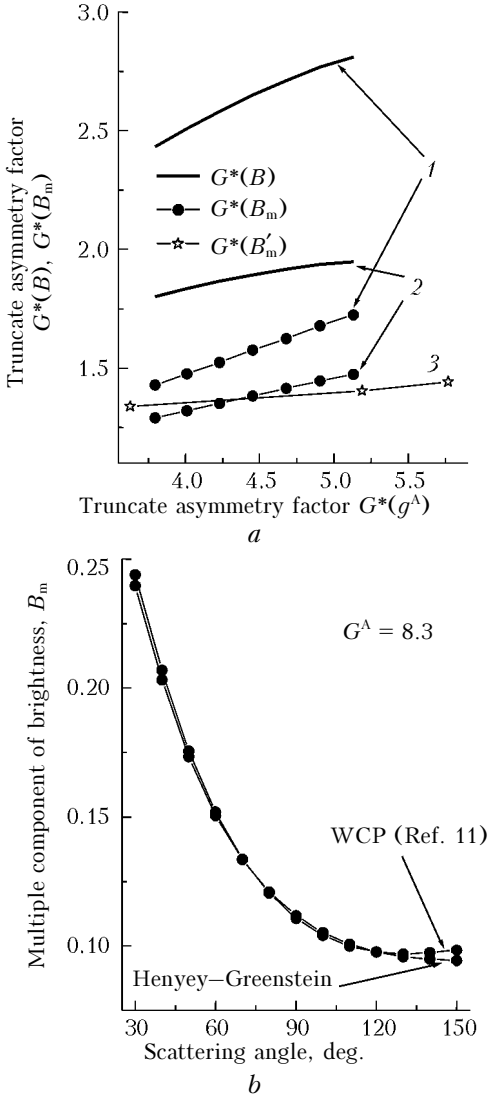

Fig. 4. Effect of elongation of the aerosol scattering phase function on the sky brightness asymmetry: dependences $G^*(B)$ and $G^*(B_m)$ on $G^*(g^A)$ for two spectral regions $\lambda = 1.25$ μm, $\tau^A = 0.1$ (*1*); $\lambda = 0.5$ μm, $\tau^A = 0.2$ (*2*) and (*3*) at $\xi = 60°$ (*a*); dependences of the brightness $B_m(\theta)$ for two types of the aerosol scattering phase functions (*b*).

With the increase of the relative characteristic τ^A/τ^R, this dependence somewhat strengthens, but the maximal change of $G^*(B_m)$ does not exceed ~15% with the change of $G^*(g^A)$ in a wide range, namely, from 3.3 to 5.2, or G^A from 5.3 to 9.7. In addition to the Henyey–Greenstein phase functions, we evaluated the $G^*(B_m) - G^*(g^A)$ relation for three different aerosol scattering phase functions mentioned in Refs. 10 and 11 (Curve *3*: $\lambda = 0.5$ μm; $\tau^A = 0.2$; G^A from 6.3 to 8.3). Calculations proved a weaker (than for the Henyey–Greenstein phase function) linear dependence of the asymmetry factor $G^*(B_m)$ on $G^*(g^A)$. In this case, the growth of the brightness asymmetry factor $G^*(B_m)$ made about 7% at a change of $G^*(g^A)$ in a wide value range 3.6–5.8.

Besides, the calculation results have shown that individual features of the aerosol scattering phase functions (except for the elongation) slightly affect the brightness component $B_m(\theta)$. This fact is illustrated in Fig. 4*b*, where angular dependences $B_m(\theta)$ are compared, which are intentionally calculated for two different scattering phase functions g^A: one of them typical for mid-latitude summer[11] and the Henyey-Greenstein function, with the same $G^A = 8.3$ for both. Maximal difference of $B_m(\theta)$ values in this example did not exceed 4% at a mean deviation of 1%.

Thus, within a preset experimental geometry (ξ; ξ) and τ^A, it is possible to make a simple parameterization of the azimuth distribution of the brightness component $B_m(\theta)$ using the linear dependence on the scattering phase function elongation $g^A(\theta)$. Specific approaches to low-parametric description of the azimuth and zenith dependences of the near-horizon sky brightness will be presented in an individual paper.

3. Dependence of sky brightness on the viewing zenith angle

In the zenith distribution of scattered radiation over the sky we can distinguish two segments, where the angular behavior of $B(\xi)$ exhibits evident distinctions. In a relatively small sector, (the principal plane, Fig. 5*a*), we observe a sharp brightness peak fading to the horizon, which is reasoned by the influence of the aureole part of the aerosol scattering phase function. The brightness decrease occurs due to increase of the scattering angle θ in the range ~0–15° while approaching the horizon ($\xi \to 90°$). The effect of the sun aureole increases with the growth of the atmospheric AOT and manifests itself even in the multiple scattering component.

Beyond the aureole, the main tendency (as was stated earlier[1–4]) is an increase in scattered radiation with the growth of the viewing zenith angle (Figs. 5*b*, *c*, and *d*). However, close to the horizon, angular dependences split in two: 1) continuous monotonic growth of sky brightness up to crossing the horizon; 2) nonmonotonic behavior of $B(\xi)$ with a peak at $\xi > 80°$ and subsequent decrease of brightness to the horizon.

According to Eq. (2), the nonmonotonic behavior of $B(\xi)$ as it approaches the horizon ($\xi \to 90°$) can be explained by a joint influence of three factors:

a) an increase in brightness with the growth of the scattering volume (the number of particles) along the viewing direction;

b) a decrease in brightness due to a greater extinction of radiation that lights the sighted atmospheric column;

c) a decrease (for the phase function in the forward hemisphere) or increase (phase function in the backward hemisphere) in brightness with the growth of the scattering angle θ due to increase of the angle ($\xi - \xi$).

The (c) factor, as is noted above, prevails only in the Sun's aureole area, where the most elongated part of the scattering phase function $g^A(\theta)$ is located. In the rest of the sky dome (Figs. 5*b*, *c*, and *d*), the character of the angular behavior of $B(\xi)$ is determined by the factors (a) and (b), which are described by the last two multipliers in Eq. (2). Depending on the optical thickness, one or other factor prevails, and the corresponding behavior of $B(\xi)$ is observed.

Consider the modification of $B(\xi)$ with τ^A changing and other parameters fixed (Fig. 5*b*). At a high atmospheric transparency ($\tau^A \to 0$), the sky brightness is minimal and grows sharply close to the horizon. As the transparency decreases ($\tau^A = 0.1$), overall sky brightness increases and a narrow peak $B_{max}(\xi_{max})$ appears near the horizon. With a further increase of AOT ($\tau^A = 0.2$), the brightness peak shifts off the horizon and becomes wider, its height going down. However, with the increase of AOT, the sky brightness in the region $\xi < \xi_{max}$ still intensifies. Such behavior of $B(\xi)$ in the near-horizon area is formed under the influence of the single and multiple scattering components, namely, their comparable contribution and qualitatively similar dependence on ξ (Fig. 5*c*).

With a change of the solar zenith angle, the regularities considered retain, but the values of B_{max} depending on τ^A may arrange in a different order. For instance, at $\xi = 85°$ (Fig. 5*d*), B_{max} monotonically decreases as the atmospheric AOT grows. Note that a change in reasonable limits of the underlying surface albedo A_S and the single scattering albedo Λ^{aer} weakly influences the character of zenith distribution of sky brightness near the horizon. To illustrate this, the asterisks in Fig. 5*b* show calculations of $B(\xi)$ for $\tau^A = 0.2$, but at $A_S = 0.4$ (instead of the standard 0.2). A considerable change of the surface albedo has intensified sky brightness by a few percent. In the case of a change of the single scattering albedo, the situation is somewhat different (see the squares in Fig. 5*d*). The growth of Λ^{aer} from 0.84 to 0.9 has intensified sky brightness in the near-horizon zone by 11.7%. At the same time, the dependence $B(\xi)$ itself and the angular position of the brightness maximum ξ_{max} remained unchanged.

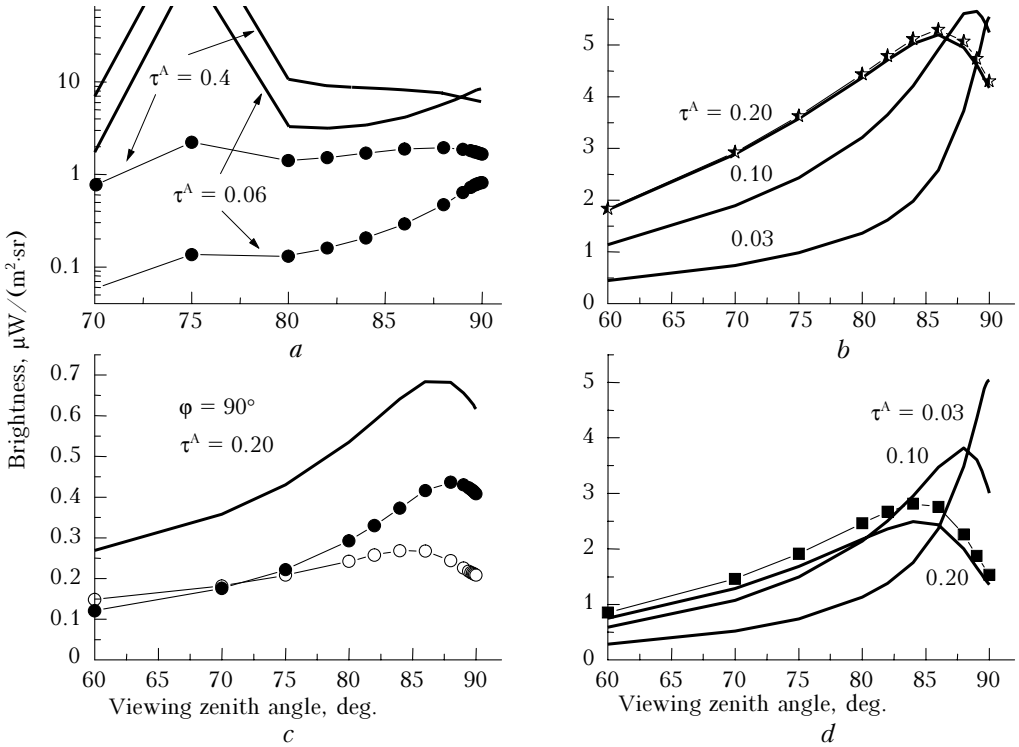

Fig. 5. Zenith dependence of sky brightness (λ = 0.87 μm) (—— for B, ○ for B_o, • for B_m): in the Sun aureole area (φ = 0°, ξ = 75°) (*a*); for different AOT values (φ = 20°, ξ = 75°) (*b*); separately for the components B_o and B_m (τ^A = 0.2, φ = 90°, ξ = 75°) (*c*); the same as (*b*), but as ξ = 85° (*d*).

The features of the angular behavior of $B(\xi)$ in different spectral regions are determined by the spectral dependence of the total optical thickness $\tau(\lambda) = \tau_\lambda^A + \tau_\lambda^R + \tau_\lambda^G$. In the visible and UV spectral regions, the value of τ is, as a rule, equal to or greater than 0.2–0.3, therefore, the maximum $B_{max}(\xi)$ covers rather wide range of angles, and the brightness decrease to the horizon starts from $\xi_{max} \approx 80°$. In the IR spectral region, due to fast fall of τ^R and then τ^A, the angular position of the brightness peak shifts to the horizon with the final value $\xi_{max} \approx 90°$. That is, $B(\xi)$ becomes a monotonically growing function over the whole range of zenith angles.

Note that the "horizon darkening" effect (decrease in brightness at about $\xi_{max} \approx 90°$) considered here was noticed earlier in the experiments, namely, in the study of the angular structure of the background brightness near the sea horizon.[12] The indicated dependence $B(\xi)$ was observed within a few degrees above the horizon both under the cloudy and cloudless conditions.

Thus, the calculations show that beyond the aureole angle region, the change of $g^A(\theta)$ and A_S is insignificant; the angular dependence of $B(\xi)$ is determined by the optical thickness, and the brightness depends also on the single scattering albedo. In other words, with the specified observation geometry (preset φ and ξ), it is possible to make a low-parameter presentation of the zenith sky brightness distribution as well as the characteristics ξ_{max} and B_{max} in the form of functions of τ^Λ and Λ^{aer} with other characteristics set in the model.

4. Refinement of the concept of scattered radiation coming from the horizon

It is of interest to analyse in a more detail the physical meaning of sky brightness immediately above the horizon B_H ($\xi \cong 90°$). The studies by the theory of the distant object visibility[13–16] the horizon sky brightness (or the haze brightness B_h) identifies with the state of "brightness saturation" for the infinite and horizontally homogeneous atmospheric layer B_∞:

$$B_h = B_\infty[1 - \exp(-\varepsilon_0 L)] \to B_\infty, \qquad (6)$$

where ε_0 is radiation extinction coefficient in the surface layer and L stands for the path length.

At the same time, it follows from the radiation transfer equation that for the plane-parallel atmosphere[5,9] the sky brightness on the horizon $B_H^*(\xi = 90°)$ is the function of medium sources:

$$B_H^* = S(\mu = 0;\varphi) = \frac{\Lambda^{atm}}{4\pi} \int_{\varphi'=0}^{2\pi} \int_{\mu'=-1}^{1} g^{atm}(\mu')B(\mu';\varphi')d\mu' d\varphi', \qquad (7)$$

where μ, μ' are the cosines of the viewing zenith angles ξ and of the spatial illumination ξ' of the path.

Naturally, the question arises to what extent the simulation results $B_H(\xi \approx 90°)$ for the spherical atmosphere (more adequate to the reality) correspond to approximation of the plane-parallel atmosphere B_H^* in the form of Eq. (7) and the presentation of the surface haze brightness saturation by Eq. (6). Analysis of this question also allows us to clarify the influence of the atmospheric sphericity on formation of the zenith distribution of sky brightness. With this purpose, within the same general approach (Ref. 6), but for the plane-parallel atmosphere we performed a numerical simulation of the brightness B_H^* ($\xi = 90°$) for different situations beyond the aureole angle region and $\xi < 82°$.

Comparative calculations have shown (Fig. 6) that, first, the character of angular dependence $B(\xi)$ (monotonic growth or decrease in brightness to the horizon) in the plane-parallel case is identical to the spherical atmosphere, and the sky brightness immediately above the horizon B_H ($\xi \to 90°$) weakly depends on the aerosol characteristics. With the increase in asymmetry of the aerosol scattering phase function G^Λ from 6.4 to 8.3 (see curves *3* and *5* in Fig. 6), the sky brightness change on the horizon did not exceed 4%. Even variations of τ^Λ in a wide range from 0.06 to 0.4 led to the B_H changes in this case only by 15%. That is, the brightness $B_H = S$ is some asymptotic value, where all angular distributions $B(\xi)$ converge, and weak dependence $B_H(\tau^\Lambda; G^\Lambda)$ is the base for obtaining simple estimates of the "horizon" brightness with the least number of preset approximate values of input parameters.

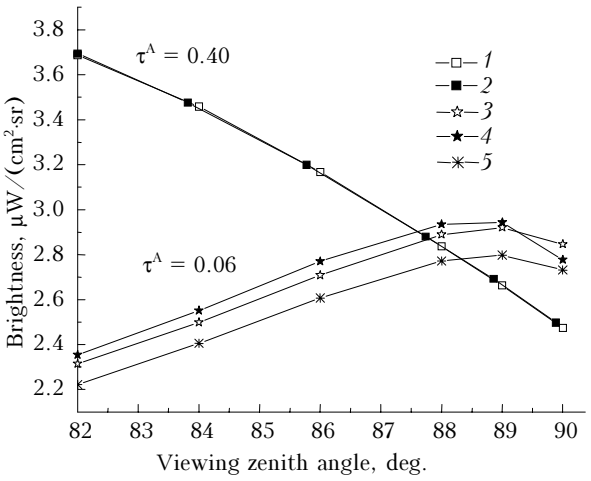

Fig. 6. Comparison of calculations of $B(\xi \to 90°)$; $\lambda = 0.5$ μm, $\varphi = 0°$) in the spherical (*1*, *3*, *5*) and plane (*2*, *4*) atmosphere for two τ^Λ and different scattering phase functions g^Λ (*1*–*4* – WCP, $G^\Lambda = 8.3$; *5* – Henyey–Greenstein function, $G^\Lambda = 6.4$).

Second, the results of two brightness calculations (for the plane and spherical atmospheres) show minor disagreements and only at small optical thicknesses. At $\tau^\Lambda = 0.06$, for example, the relative difference $\delta_1 = [B(\xi) - B^*(\xi)]/B(\xi)$ for the near-horizon sky brightness does not exceed 2%. A more thorough comparison (for different τ^Λ, φ, ξ) of the characteristic δ_1 is made for the sky brightness immediately above the horizon (Table 2).

Table 2. Comparison of calculations of the sky brightness above the horizon for spherical and plane-parallel atmospheres

λ, μm	τ^Λ	ξ, °	φ, °	B_H, μW/(cm²·sr)	B_H^*, μW/(cm²·sr)	δ_1, %
0.5	0.06	60	0	2.85	2.78	2.4
0.5	0.06	60	90	0.803	0.792	1.4
0.5	0.06	60	180	0.886	0.872	1.6
0.5	0.4	60	0	2.47	2.47	0.2
0.5	0.4	60	90	0.684	0.685	−1.4
0.5	0.4	60	180	0.586	0.588	−0.3
0.87	0.03	75	20	5.55	5.71	−3.0
0.87	0.03	75	90	0.707	0.714	−1.0
0.87	0.03	85	20	5.04	0.484	4.1
0.87	0.03	85	90	0.484	0.459	5.2
0.87	0.1	75	20	5.24	5.17	1.4
0.87	0.1	75	90	0.672	0.669	0.5
0.87	0.1	85	20	3.01	2.76	8.4
0.87	0.1	85	90	0.319	0.304	4.7
0.87	0.2	75	20	4.17	4.13	1.0
0.87	0.2	75	90	0.617	0.615	0.3
0.87	0.2	85	20	1.35	1.24	8.8
0.87	0.2	85	90	0.208	0.198	4.6

From the results given it follows that δ_1 becomes as large as 4% and greater only near the solar aureole and at $\xi > 82°$. Beyond the solar aureole, the disagreement $(B_H - B_H^*)$ becomes insignificant at $(\tau^\Lambda + \tau^R > 0.2)$. This estimate only slightly differs from the data in Ref. 5 (Section 4, Fig. 3), where similar calculations were performed for another viewing angle $\xi = 89°$ without accounting for absorption.

The analysis of the close problem on the brightness saturation of the atmospheric haze on horizontal paths[14–16] enabled the assumption that the criterion "insignificant brightness disagreement" is more correct to be determined as dependent on the thickness τ^*, which comes up within the homogeneous surface layer at observation of sky on the horizon rather than on the vertical thickness τ. With allowance for the horizon observation geometry in the spherical atmosphere,[17,18] τ^* can be written as:

$$\tau^* = \varepsilon_0 L(\xi; h; h_0) \approx \varepsilon_0 (38.9 + 123\sqrt{h}), \qquad (8)$$

where L is the path length, in km, within the surface layer; h is the observation point height, in km; $h_0 \approx 0.1$ km is the surface layer height.

Indeed, when sighting the horizon ($\xi \to 90°$), the sky brightness is essentially formed by optical properties of the surface layer. Therefore, as the atmospheric haze brightness approaches the state of saturation [Eq. (6)], the brightness disagreement $(B_H - B_H^*)$ must go down as well. To prove it, let us consider calculation results for $\delta_1(\tau^*)$ and $\delta_2 = (B_\infty - B_h)/B_\infty = \exp(-\varepsilon_0 L)$ that characterize the brightness saturation of the atmospheric haze (Fig. 7).

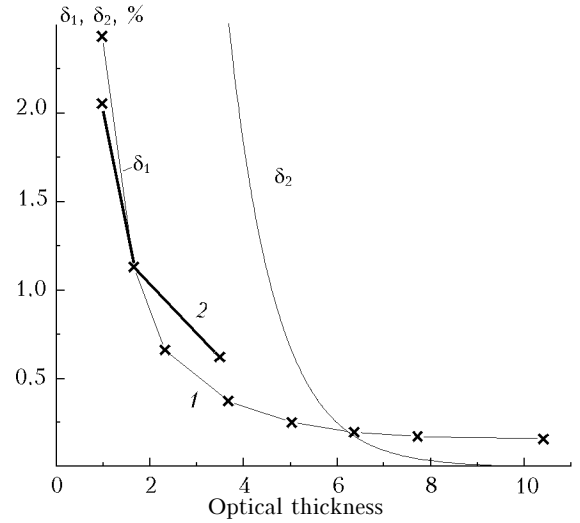

Fig. 7. Dependence of the relative distinctions δ_1, δ_2 on the optical thickness τ^*, within the surface layer (100 m) in observations of the horizon.

Note that quantitative agreement between the results is not to be expected since in these examples somewhat different situations are simulated:

a) the parameter δ_2 describes the brightness increase $B_h(L) \to B_\infty$ of the horizontal near-ground atmospheric column bounded by a black screen at a changing L (Refs. 13–16);

b) in calculations of δ_1 not only the surface brightness, but that of all the above lying layers is taken into account.

Figure 7 shows that the dependence $\delta_1(\tau^*)$ is close to the exponential function $\delta_2(\tau^*)$, but, because of "extra brightness", it is shifted to the range of lower τ^* values. In the considered calculations of $\delta_1(\tau^*)$ (curve *1*), optical thickness $\tau^* = \varepsilon_0 L$ varied due to changes in the vertical thickness τ (from 0.05 to 0.4) and the respective change of ε_0. In another variant (curve *2*), calculation of the brightnesses B_H, B_H^*, and the corresponding values of $\delta_1(\tau^*)$ was performed for the aerosol model, where the extinction coefficient ε_0 varied from 0.03–0.1, while vertical thickness was fixed ($\tau^\Lambda = 0.075$). A good agreement between the calculation results (curves *1* and *2*) indicates that δ_1 is indeed determined by the degree of turbidity of the atmospheric surface layer, and at $\tau^* > 2$ (or $\varepsilon_0 > 0.035$ and observation height $h = 20$ m) the difference between B_H and $B_H^* = S$ does not exceed 1%. For observations in the visible spectral region this requirement corresponds to the visibility range up to 100 km, i.e., covers the majority of realistic situations.

This inference is important for one more question. In various problems of atmospheric optics, with the increase in zenith angles ξ and ξ, the necessity of allowance for refraction increases as well. In this case, for the sky brightness above the horizon beyond the solar aureole and not large ξ, the fulfillment of the brightness saturation requirement for the haze excludes the necessity of regarding the refraction. This follows just from the fact of proximity of B_H and B_H^* values, which are equivalent to conditions with different terrestrial refraction coefficients: calculations of B_H are performed for the spherical atmosphere regardless of refraction (i.e., the refraction coefficient $k = 0$). Calculation of B_H^* for the plane atmosphere actually corresponds to $k = 1$. However, to meet the requirement $\tau^* > 2$, the path length $L(\xi; h; h_0)$ in the surface layer must be evaluated with allowance for refraction.

Conclusion

We have analyzed regularities of formation of the spatial-angular structure of the clear-sky brightness in transparency windows in the visible and near-IR spectral regions based on numerical simulation of the scattered solar radiation with allowance for atmospheric sphericity and molecular absorption. Thus, we can make the following main conclusions:

1. The sky brightness field in the region of large zenith angles ($\xi \sim 60$–$90°$) is formed at comparable contributions (under standard conditions) of the singly scattered solar radiation and multiply scattered radiation incoming from the upper and lower hemispheres. The angular brightness distribution $B(\xi; \varphi)$ with elongation to the Sun and the near-horizon zone is mainly determined by the single component B_o; the multiple component B_m is qualitatively similar in behavior, but differs in its much less asymmetry. Redistribution of the contributions of the single and multiple scattering occurs with the change (in the order of significance) of the angle θ, the characteristic τ^Λ, elongation of the aerosol scattering phase function, and the solar zenith angle.

2. Azimuth behavior of the sky brightness in different almucantars depends first of all on the atmospheric scattering phase function $g^{atm}(\theta)$, which undergoes a joint influence of the aerosol and molecular scattering. The single brightness component with accuracy to the constant follows $g^{atm}(\theta)$, while the multiple one has a weak and almost linear dependence on elongation of the aerosol scattering phase function. At variation of the types and elongation of $g^\Lambda(\theta)$ in the wide value range, a change of the brightness asymmetry factor $G^*(B_m)$ is about 7% at the average of 1.4. The main brightness variability (5–10 times and more) is observed in the forward hemisphere due to priority of the more asymmetric aerosol scattering phase function and single scattering. Angular dependence of sky brightness in the backward hemisphere is determined by the multiple component and molecular scattering, so the change of $B(\theta)$ is, as a rule, below 100%. Redistribution of contributions of the aerosol and molecular, single and multiple scattering occurs at $\theta \approx 60°$.

3. The zenith distribution of the sky brightness (beyond the solar aureole area) has the form of a nonmonotonic function with a peak at $\xi = 80$–$90°$, whose characteristics (B_{max}, ξ_{max}) depend on the

optical thickness $(\tau^{\Lambda} + \tau^{R})$. Variations of the scattering phase function $g^{\Lambda}(\theta)$, A_S, and Λ^{aer} weakly influence the character of the dependence $B(\xi)$. The earlier noted regularity of the monotonic increase of the sky brightness to the horizon is in fact a particular case of the high atmospheric transparency conditions (since $\xi_{max} \to 90°$ at $\tau \to 0$). Disagreement between the brightness $B(\xi)$ calculations for the spherical and plane-parallel atmospheres at $\tau > 0.2$ does not exceed 1%.

4. As approaching the horizon, angular distributions of $B(\xi)$ converge asymptotically to the value $B_H = S$ as a result of brightness saturation of the surface haze. For most observation cases ($\xi < 82°$, $\varphi > 30°$, $\varepsilon_0 > 0.04$), the sky brightness on the horizon $B_H(\varphi)$ is resistant to the changes in atmospheric conditions and can be parameterized in the form of dependence on the approximate τ^{Λ} values and the elongation of the aerosol scattering phase function.

5. Transformation of the sky brightness field with the wavelength growth is determined by the spectral dependence of the total thickness $(\tau^{\Lambda} + \tau^{R})$ and the relative characteristic $(\tau^{\Lambda}/\tau^{R}) \sim \lambda^{-3}$: the total brightness level and the role of the multiple component decrease asymptotically; the azimuth dependence becomes more elongated; the maximum in the zenith distribution of the sky brightness shifts towards the horizon.

Acknowledgments

This work is supported in part by the Russian Foundation for Basic Research (grant No. 02–05–64492) and DOE's ARM program (contract No. 5012).

References

1. E.V. Pyaskovskaya-Fesenkova, *Investigation of Light Scattering in the Earth's Atmosphere* (USSR Academy of Sciences Press, Moscow, 1957), 219 pp.
2. K.S. Shifrin and N.P. Pyatovskaya, *Tables of Slant Visibility and Daylight Sky Brightness* (Gidrometeoizdat, Leningrad, 1959), 210 pp.
3. V.I. Kushpil', *Clear Daylight Sky Brightness (Experimental Data)* (ONTI GOI, Leningrad, 1971), 164 pp.
4. K.Ya. Kondratyev, ed., *Radiation Characteristics of the Atmosphere and Earth Surface* (Gidrometeoizdat, Leningrad, 1969), 564 pp.
5. T.B. Zhuravleva, I.M. Nasretdinov, and S.M. Sakerin, Atmos. Oceanic Opt. **16**, Nos. 5–6, 496–504 (2003).
6. T.B. Zhuravleva, I.M. Nasretdinov, S.M. Sakerin, K.M. Firsov, and T.Yu. Chesnokova, Atmos. Oceanic Opt. **16**, No. 12, 972–981 (2003).
7. G. Anderson, S. Clough, F. Kneizys, J. Chetwynd, and E. Shettle, *AFGL Atmospheric Constituent Profiles* (0–120 km), Air Force Geophysics Laboratory, AFGL-TR-86-0110, Environmental Research, Paper No. 954 (1986).
8. V.A. Smerkalov, *Applied Atmospheric Optics* (Gidrometeoizdat, St. Petersburg, 1997), 334 pp.
9. J. Lenoble, ed., *Radiative Transfer in Scattering and Absorbing Atmospheres. Standard Computational Procedures* (Deepak, Hampton, 1985).
10. V.A. Smerkalov, Atmos. Oceanic Opt. **13**, No. 4, 293–298 (2000).
11. *A Preliminary Cloudless Standard Atmosphere for Radiation Computation.* World Climate Research Programme. WCP-112, WMO/TD No. 24 (1986), 60 pp.
12. M.V. Kabanov and S.M. Sakerin, *On the Sea-Horizon Background Radiation Brightness*, in: *III All-Union Meeting on the Atmospheric Optics and Actinometry,* Tomsk (1983), Part I, pp. 181–183.
13. V.V. Sharonov, *Calculation and Measurement of Distant Object Visibility* (Gostekhizdat, Moscow, 1947), 284 pp.
14. V.A. Gavrilov, *Atmospheric Visibility* (Gidrometeoizdat, Leningrad, 1966), 323 pp.
15. I.A. Savikovsky, Tr. Gl. Geofiz. Obs., Issue 240, 168–181 (1969).
16. V.A. Kovalev, *Atmospheric Visibility and Its Definition* (Gidrometeoizdat, Leningrad, 1988), 216 pp.
17. M.V. Kabanov and S.M. Sakerin, Izv. Akad. Nauk SSSR, Fiz. Atmos. Okeana **18**, No. 7, 711–719 (1982).
18. K.V. Kazansky, *Terrestrial Refraction over Wide Water Surfaces* (Gidrometeoizdat, Leningrad, 1966), 192 pp.